

Gulf Stream and ENSO Increase the Temperature Sensitivity of Atlantic Tropical Cyclones

J. C. MOORE

Arctic Centre, University of Lapland, Rovaniemi, Finland

A. GRINSTED

Arctic Centre, University of Lapland, Rovaniemi, and Department of Geophysics, University of Oulu, Oulu, Finland

S. JEVREJEVA

Proudman Oceanographic Laboratory, Liverpool, United Kingdom

(Manuscript received 1 November 2006, in final form 21 May 2007)

ABSTRACT

Controversy exists over the role of the recent rise in sea surface temperatures (SST) and the frequency of tropical cyclones or hurricanes. Here, 135 yr of observational records are used to demonstrate how sea surface temperature, sea level pressure, and cyclone numbers are linked. A novel wavelet-lag coherence method is used to study cause and effect relations over a large space of time scales, phase lags, and periods. It is found that SST and cyclones are not merely correlated, but are in a negative feedback loop, where rising SST causes increased numbers of cyclones, which reduce SST. This is statistically most significant at decadal and not at longer periods, which is contrary to expectations if long-period natural cycles are important in driving cyclone numbers. Spatial relationships are examined using phase-aware teleconnections, which at the dominant decadal period show the in-phase behavior of the Atlantic SST in the Gulf Stream region, reflecting the role of the transportation of heat northward from the tropical Atlantic. At 5-yr periods there is significant coherence when SST leads cyclones by 2 yr, and this is associated with tropical ENSO activity such that, as predicted, increasing numbers of El Niños cause fewer Atlantic cyclones. The pattern of coherence existing since 1970 strongly favors the decadal coherence band, and despite growing coherence at higher frequencies, there is none at the 5-yr band, perhaps explaining why the observed sensitivity between SST and cyclones is larger than that from general circulation model (GCM) predictions and becoming greater.

1. Introduction

The nature of the link between hurricanes and the rising global temperatures is controversial (Goldenberg et al. 2001; Emanuel 2005; Landsea 2005; Landsea et al. 2006; Mann and Emanuel 2006; Elsner 2006) and difficult to ascertain because hurricanes are rare events at the statistical tail of the wind speed distribution found in nature (Landsea 2005; Landsea et al. 2006). Some authors have claimed that there are too many uncertainties in the observational record to detect any changes in hurricane frequency (Landsea et al. 2006) or

that those fluctuations may be driven by multidecadal natural cycles (Goldenberg et al. 2001) or, alternatively, that they may be driven by global air temperatures (Emanuel 2005; Elsner 2006). Other studies have highlighted the complex problem of predicting hurricane numbers using synoptic-scale observations (Michaels et al. 2006) or general circulation model (GCM) simulations (Knutson and Tuleya 2004), concluding that any dependence of hurricane numbers on anthropogenic global warming is small and within the uncertainty limits. It is known that weak teleconnections exist between the Atlantic hurricane source region and the northern Atlantic (Goldenberg et al. 2001) and tropical Pacific warm pools (Wang et al. 2006).

However, robust linkages that may imply causal relationships between global sea surface temperature

Corresponding author address: J. C. Moore, Arctic Centre, University of Lapland, Pohjoisranta 4, Rovaniemi 96200, Finland.
E-mail: jmoore@ulapland.fi

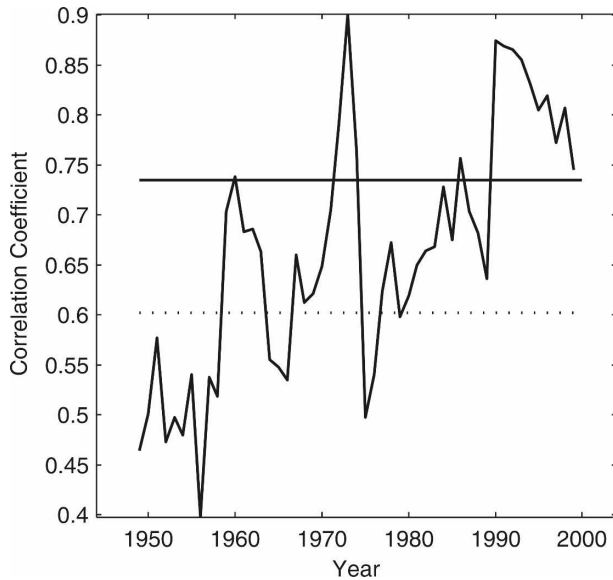


FIG. 1. Correlation between PDI and TC in 10-yr moving windows. The 1% (solid line) and 5% (dotted line) significance levels are shown.

(SST), pressure fields, and cyclones have not been established. Challenging the identification of such linkages are both the uncertainties in long-term observational records and the need for advanced statistical methods designed specifically to extract possibly causal relationships that may be nonstationary and develop over many years. Here we apply advanced frequency-domain wavelets to a 135-yr observational record and demonstrate how SST, sea level pressure (SLP), and cyclone numbers are linked on different time scales.

2. Data

One way of collecting a long, reasonably reliable record without the difficulties associated with measuring wind speed is to use the numbers of Atlantic tropical cyclones per year (TCs), as they are defined simply as nonfrontal, synoptic-scale cyclones over tropical or subtropical waters (Jarvinen et al. 1984). We use TC to represent the cyclone count and the power dissipation index (PDI) (Emanuel 2005; Landsea 2005), an index of hurricane destructive power available from 1944 to 2004, are correlated at 0.68. Figure 1 shows the correlation between PDI and TC has varied over time, but for much of the common period of data the correlation is significant at the 95% level, with only the period prior to 1955 showing consistently lower significance. The TC record from ship observations and later from aircraft and satellite observations extends back to 1851 (Jarvinen et al. 1984). Ship observations increase in number

backward in time, and the routes traveled were more varied than today, so although some storms must have been missed, they were less able to avoid cyclones than at present. The moving correlation between TC and PDI (Fig. 1) suggests that we can use TC as a surrogate with reasonable confidence, though the earlier part of the record is certainly likely to be less reliable than that of the postsatellite era. Recent modifications to TC have been suggested (summarized by Mann et al. 2007); however, testing our results with the proposed time-varying bias added to TC makes only very slight differences to our results. For example, the correlation coefficient between PDI and TC changes from 0.68 to 0.69. Because there are probably as good reasons to doubt the “corrections” as the original TC time series (Mann et al. 2007), we use only the original TC. The long TC record allows more rigorous significance testing for long-period variability than analyses that have focused on the instrumental records available only from the 1940s or later (Emanuel 2005; Michaels et al. 2006). While this approach seems to work well for the Atlantic, it is less likely to be applicable in areas with less shipping, so the global record of tropical cyclones may be more difficult to confidently establish.

We consider the set of SSTs for the Atlantic averaged over the area 6° – 18° N, 20° – 60° W, defined as the cyclone main development region (MDR), during the months of August–October (SST_C). We use the Hadley Centre Global Sea Ice and Sea Surface Temperature (HadISST) data (Rayner et al. 2003), which extend from 1870 to 2004, though the analyses are not sensitive to alternative SST reconstructions (e.g., Smith and Reynolds 2004). Observational evidence supports a link between the maximum storm wind speed and the maximum SST along its track in the MDR (Michaels et al. 2006; Wang et al. 2006); the relationship however is nonstationary and suggestive of various complicating factors in hurricane development (Michaels et al. 2006), such as lapse rates, vertical wind shear, and moisture characteristics. There is a well-established theory (potential intensity) that shows that the thermodynamic control of tropical cyclone intensity is a function of the air–sea disequilibrium (which is a function of the SST) and the ability of this enthalpy extracted from the ocean to be convected through the troposphere (Emanuel 1986, 1988). There is, however, no theory that predicts the number of Atlantic tropical storms as a function of SST (or potential intensity). GCM simulations suggest that there is a link between rising SST and the strength of the hurricane maximum wind speed, such that a 1° C rise in SST_C leads to a 5% increase in maximum wind speed (Knutson and Tuleya 2004). However, observations in the Atlantic region suggest

that the PDI, which is dominated by the largest storms, has increased by about 20% °C⁻¹ since 1980, and perhaps by 10% °C⁻¹ over the twentieth century (Emanuel 2005; Landsea 2005).

3. Methods

In this paper we often refer to “causality,” by which we really mean Granger causality (Granger 1969; Elsner 2006). A variable X is said to Granger cause a variable Y if it can be shown that time series values of X provide significantly improved predictions of future values of Y than predictions based on Y alone would. Ideally, but in practice quite seldom, it is found that one time series is a useful predictor of the other, but not vice versa. All of the relationships we find in this paper exhibit strong Granger causality; that is, the causality relation applies in only one direction. By this we mean that only one of the two time series appears to be a significant predictor of the other; hence, they are stronger tests of causality than the standard Granger causality test. It is, however, possible that both variables X and Y may be “caused” by another parameter. The tests we develop are based on wavelet filtering the time series and are quite different from Granger causality, which relies on regression between lagged versions of two time series.

Wavelet transforms expand time series into time–frequency space and can therefore find localized intermittent periodicities; wavelet coherence examines localized correlations in time–frequency space between two different time series. Wavelet coherence is useful because relative phase relationships between two time series over a wide spectrum of temporal scales are produced (Grinsted et al. 2004; Moore et al. 2006).

We use the continuous wavelet transform (CWT) with two different wavelets. The idea behind the CWT is to apply the wavelet as a bandpass filter to the time series. Here, we use two different wavelet types that have different properties in time–frequency space. For broad bandpass-filtering applications, we use the Paul wavelet of order 4 defined by its Fourier wavelength, λ . The Paul wavelet is not very localized in frequency space (Torrence and Compo 1998), as it is a broad bandwidth filter. Thus, it allows signals that are relatively aperiodic to be included in the analysis, and it also makes the results we show very robust over a large range of λ . In contrast to the broadband, but temporally narrow, Paul wavelet, the Morlet wavelet provides a good balance between time and frequency localization and is a good choice for feature extraction in general time–frequency domain plots, and so we use it in the wavelet coherence analysis (Grinsted et al. 2004). The

definition of wavelet coherence closely resembles that of a traditional correlation coefficient, and it is useful to think of it as a localized correlation coefficient in time–frequency space. We apply significance testing by Monte Carlo methods with a red noise model based on the autocorrelation functions of the two time series (Grinsted et al. 2004).

The CWT, W_n^X , of a time series X , ($x_n, n = 1, \dots, N$), with uniform time steps δt , is defined as the convolution of x_n with the scaled and normalized wavelet. The complex argument of W_n^X can be interpreted as the phases of $X(\phi_1, \dots, \phi_n)$. We consider nonlinear interactions between the two time series that may be chaotic by analyzing the phase expression of the time series derived with the Paul wavelet. A measure of the coherence between two time series, X, Y , with their respective phases ϕ and θ , is the angle strength of the phase angle difference between the series, also known as the mean phase coherence (Mokhov and Smirnov 2006), ρ :

$$\rho = \frac{1}{N} \sqrt{\left[\sum_{t=1}^N \cos(\phi_t - \theta_t) \right]^2 + \left[\sum_{t=1}^N \sin(\phi_t - \theta_t) \right]^2} \quad (1)$$

Typo corrected.

This is a measure of the variability in the phase lag between X and Y . We can search for the optimum relative phase delay between the two series by lagging one time series relative to the other by a phase lag, Δ , in (1). Inconsistencies in measurement procedures during the cyclone observational period (Landsea et al. 2006) are unlikely to introduce coherent systematic changes in the phase difference. Hence, ρ is a more robust indicator than simple correlation or linear regression.

The results can be visualized in a two-dimensional plot of ρ in period–lag (λ – Δ) space analogous to the wavelet frequency–time space plot. As a further refinement in the utility of such a plot, we find it useful to contour the strength of the linear regression of the wavelet filtered time series as a function of λ and Δ , so that the color-scale bar corresponds to the value of the coefficient m in the equation of

$$W_Y(\lambda, t + \Delta) = m W_X(\lambda, t). \quad (2)$$

The data boundaries are considered by computing a cone of influence (Torrence and Compo 1998), and data affected are excluded in the computation of ρ and m as a function of λ and Δ . The phase relationship over the range of multiyear to decadal periods was examined by filtering both time series with Paul wavelets having λ between a high-frequency limit determined by the Nyquist frequency and a low-frequency cutoff of 40 yr. The wavelength space was filled with six values of λ per

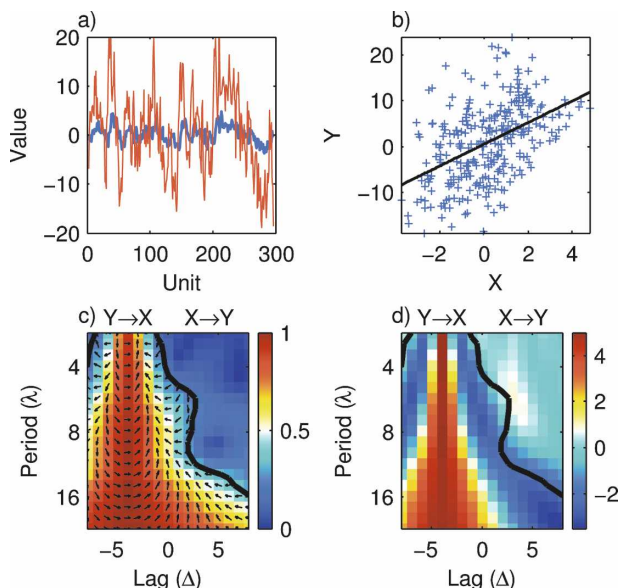


FIG. 2. (a) Plot of X and Y red noise data. (b) Scatterplot of x and y data and the linear best fit the data: $Y = 2.4X + 0.5$. (c) The wavelet lag coherence plot showing values of mean phase coherence (ρ) and its 95% confidence interval (solid black contour). (d) The sensitivity, m , in Eq. (2) for the same data. The confidence interval shown is that for ρ . The arrow notation in $Y \rightarrow X$, etc., denotes that Y leads X in lag space.

octave of scale. Significance was calculated by Monte Carlo methods with 1000 surrogate series pairs having the same red noise characteristics as the two data series.

Figure 2 illustrates the method using series where the X is red noise with a first-order autoregressive coefficient of 0.8, mean of zero and unit variance, and series Y and equal to $5X$ plus white noise (zero mean, unit variance). Then, X is lagged by four time units relative to Y , so that in our sense Y leads and hence is Granger causative of X . Figure 2a shows X and Y , and Fig. 2b is their scatterplot with the linear best fit to the data: $Y = 2.4X + 0.5$, which fails to capture any important linkage between the two noisy series. Figure 2c is the wavelet lag coherence plot showing values of mean phase coherence (ρ) and its 95% confidence interval by the solid black contour. Note that the arrows points to the right at a lag of -4 indicating that is when X and Y are in phase at all λ . The lag where the in-phase relation occurs is -4 , and the labeling above the negative lag part of the abscissa ($Y \rightarrow X$) denotes that Y predicts X , or equivalently that Y Granger causes X . Figure 2d plots the sensitivity, m , in Eq. (2) for the same data. Note that the value of m is 5 at a lag of -4 for all λ , which is exactly as expected from the construction of X and Y , and quite different from the simple regression fit. The value of m varies at all other lags than -4 , with a broadening of features at longer λ as the absolute value of Δ

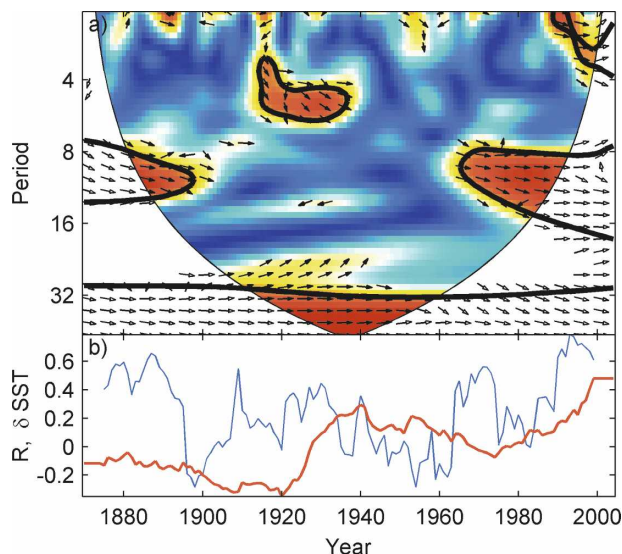


FIG. 3. (a) Squared wavelet coherence between SST_C and TC (red, high values; blue, low values). The 5% significance level against red noise is shown as a thick contour. The relative phase relationship is shown as arrows (with in-phase pointing right, antiphase pointing left, and SST_C leading TC by 90° pointing straight down); the curved lines with no coloring delineate the region affected by data boundaries (Grinsted et al. 2004). (b) The running correlation (thin line) and SST_C deviation from its mean (thick line) with 10-yr windows.

is a smaller fraction of λ . Similarly, the direction of the arrows in Fig. 2c because the angular phase lag represented by Δ varies with λ . This means that the value of m will change sign if the lag is longer than half of the period. To determine which values of m are significant, we use the confidence interval of ρ (shown in Figs. 2c and 2d) as this defines the region of λ - Δ space where the values of m have true predictive value; plotting the confidence interval of m would merely show those regions where m was significantly different from 0.

4. Results and discussion

a. Wavelet coherence

The wavelet coherence between SST_C (i.e., August–October MDR SST) and TC (Fig. 3) shows that before 1910 and since 1970 the dominant coherence has been at decadal periods. Between 1920 and 1940, coherence was at about 5-yr periodicities. Between 1910 and 1920 and again between 1940 and 1970, there was little coherence and low values of correlation. The phase relationship indicates that SST_C leads TC, and suggests that it is temperatures that drive cyclone numbers. The generally high values of the correlation coefficient between 1920 and 1940 are curious; we have no adequate explanation for the higher values, but note that during the

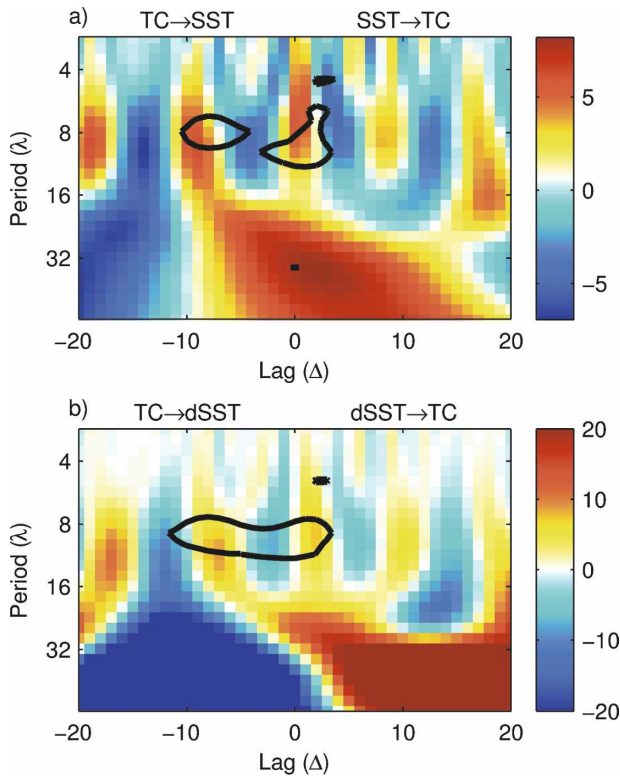


FIG. 4. (a) The TC sensitivity on SST_C (m , in number per $^{\circ}C$ on color bar) as a function of Paul wavelet filtered period (λ) and phase lag (Δ); contours and arrows as in Fig. 2. (b) As in the (a), but with TC and the $dSST_C$.

same time period the North Atlantic Oscillation (NAO) and the Arctic Oscillation were unusually uncorrelated (Jevrejeva and Moore 2001), suggesting that the Atlantic sector circulation patterns may have been reorganizing during this period.

b. Wavelet-lag regressions

We examine more closely the relative phasing of the SST_C and TC in λ - Δ space (Fig. 4). The dominating feature in Fig. 4 is the decadal wave structure, especially at $\Delta < 0$. There is significant coherence when SST_C leads TC by 0–2 yr at decadal periods. This means that SST_C can predict TC in the decadal band and from the regression we see that two to four more cyclones per degree Celsius are expected. This result is consistent with the relationships Elsner (2006) found between global air temperatures and PDI, which is an integrated measure of storm activity and intensity. The region of significance in Fig. 4 where TC leads SST_C contains both positive and negative values of m where the lag goes through a complete cycle of λ . We do not consider this convincing evidence for TC predicting SST_C as there is no consistent positive or negative value of m ,

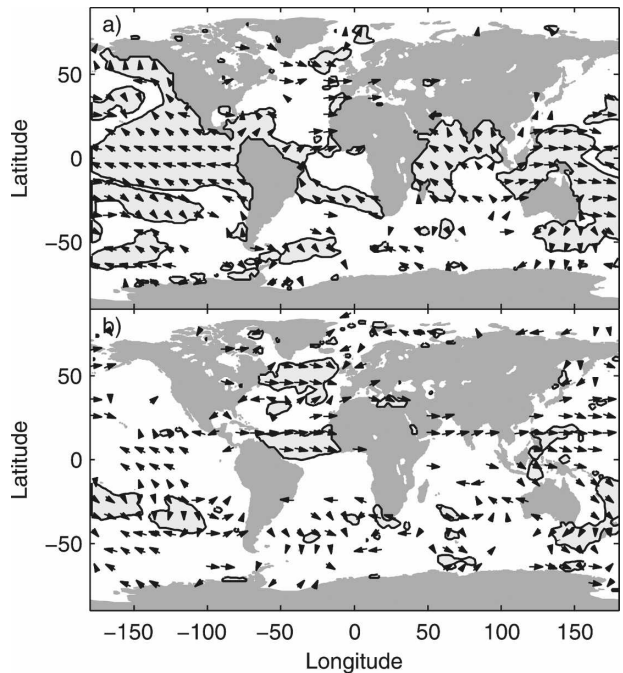


FIG. 5. Phase-aware teleconnections between TC and global SST, with arrow directions as in Fig. 3, and 95% significant areas outlined in gray at (a) 5-yr and (b) decadal periods.

but it is perhaps suggestive of a more complex interaction between the two series that we investigate next. Figure 4 also shows the λ - Δ plot of TC against the time derivative of SST_C ($dSST_C$); when TC is leading, there is a tendency to lower SST_C , at lags of less than 5 yr for decadal cycles. There is also a significant positive value of m for positive lags, and zero m at a lag of 0. The plot is therefore quite different from the left-hand panel in Fig. 4. Taken together these features are evidence for a negative feedback loop between SST_C and TC, whereby increasing SST_C raises TC, but this then leads to lower $dSST_C$, hence slowing the rise of SST_C .

Although SST_C and TC are positively correlated at all scales, at long periods, which should be related to the Atlantic multidecadal oscillation (AMO), there is no significant region of ρ , which indicates that there is no causative relationship between AMO-driven SST_C and TC. This is consistent with the discussion in the previous paragraph, and with the idea that global temperatures drive PDI and TC (Mann and Emanuel 2006; Elsner 2006). This also contradicts the suggestion (Goldenberg et al. 2001) that long-period Atlantic cyclicity is a significant hurricane forcing mechanism. The 95% significant area of ρ at λ of 5 yr has negative values of m , implying that higher SST_C causes fewer tropical cyclones on these scales, in contrast with the decadal period results.

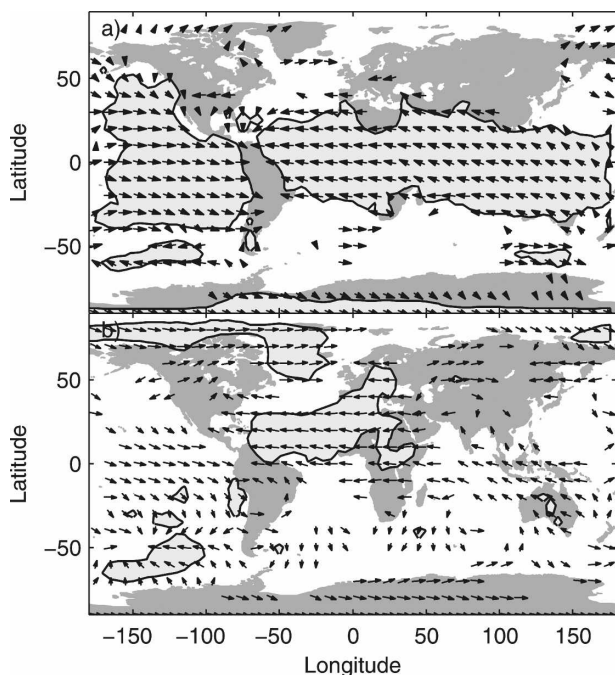


FIG. 6. Phase-aware teleconnections between TC and global SLP, with arrow directions as in Fig. 3, and 95% significant areas outlined in gray at (a) 5-yr and (b) decadal periods.

c. Phase-aware teleconnections

We next consider teleconnections between TC and the global SST and SLP fields. The phase coherence (ρ) and the average relative phase between SST in a grid cell and the Paul wavelet filtered (at Fourier wavelength λ) TC are calculated. In this way we plot regions of significant coherence (defined by ρ) and the relative lag (defined as an angle) within these regions. Figure 5 shows the phase-aware teleconnection pattern with $\lambda = 5$ and 10 yr between the TC signal and the global SST field (taken from Smith and Reynolds 2004). The arrows indicate the relative phase angle and the heavy black lines the regions where ρ is significant. The difference between the two λ s is very clear, with the tropical regions generally being in phase and highly significant at 5-yr periodicity, while it is small extratropical areas that are significant (and in phase) at decadal periods.

Figure 6 shows the phase-aware teleconnections between TC and global SLP (Allan and Ansell 2006). Note the tropical significant region for the 5-yr filtered signals. The significant region for decadal signals is both the MDR and the North Atlantic. We searched for an external driver for the decadal variability by examining coherence during intervals when decadal periodicity was strong (1870–1900 and 1970–2005), between TC and the Southern Oscillation index (Ropelewski and Jones 1987) (yearly and October–December val-

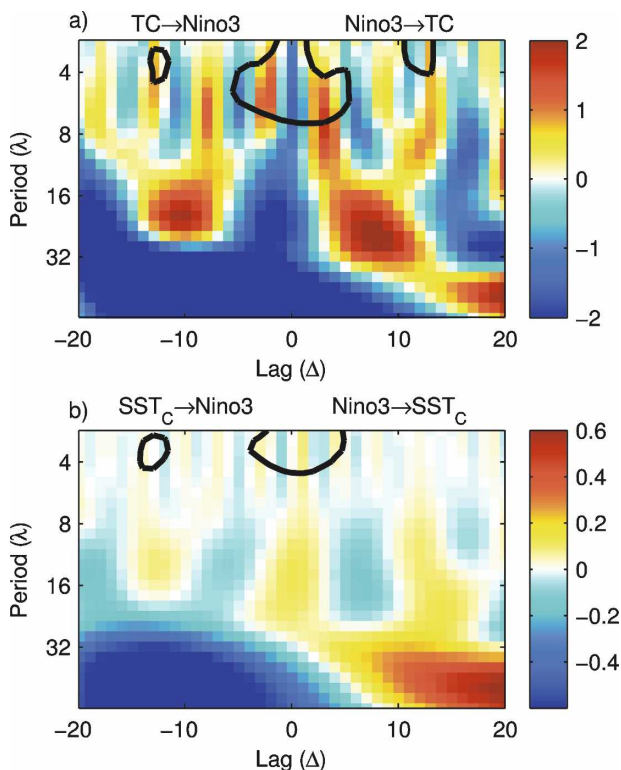


FIG. 7. As in Fig. 4 but for (a) TC sensitivity on Niño-3 (November–December) and for (b) Niño-3 (November–December) sensitivity on SST_C .

ues), the NAO (Jones et al. 1997), the Indian Ocean dipole [information online at <http://www.jamstec.go.jp/frsgc/research/d1/iod/>], the Pacific decadal oscillation (Zhang et al. 1997), the global SST (Smith and Reynolds 2004), and the sunspot number (information online at <http://sidc.oma.be/DATA/monthssn.dat>). None gave a common coherence in the 10-yr band. As there are no correlations between the obvious candidates for external forcing of TC, the notion that the linkages and phase relationships found for TC with SST and SLP do indeed represent a causative relationship in the more general meaning than purely Granger causality appears to be convincing.

d. 5-yr variability

Because the 5-yr teleconnection appears to have an ENSO-like pattern, we show the λ, Δ plot for tropical Pacific SST [we use Niño-3 (Kaplan et al. 1998), November–December anomalies as they are most decisive (Wang et al. 2006)]. There is significant ρ between TC and Niño-3 at λ of 5 yr (Fig. 7); the relationship between SST_C and Niño-3 is much less pronounced (Fig. 7b) and has very low values of m . This suggests a nonoceanic teleconnection, likely relying on an atmo-

spheric bridge such as precipitation or wave propagation as supported by the SLP TC relationship (Fig. 6). An atmospheric bridge would probably require short phase lags, on the order of months, which is consistent with the lower end of the observed phase lag range of 0–2 yr (Fig. 4).

Tsonis et al. (2005) showed that global warming likely leads to an increased frequency of El Niño. Wang et al. (2006) conclude that an increase in Atlantic hurricane activity requires a decrease of SLP and increases in atmospheric convection and cloudiness, which corresponds to a weak tropospheric vertical wind shear and a deep warm upper ocean. El Niño is associated with low air pressure over the central and eastern Pacific Ocean, and from the TC–SLP 5-yr map, this corresponds to an increase in SLP over the Atlantic MDR region. This is consistent with $m < 0$ in Fig. 4 for $\lambda = 5$ yr, indicating that increasing the frequency of El Niño conditions tends to reduce the Atlantic TC count. However, recent decades are marked by TC SST_C coherence at decadal and at 2–3-yr periods, but not in the 5-yr band (Fig. 3), as may be expected with the increasing frequency of El Niño over the last 40 yr (Tsonis et al. 2005). We can speculate on two possible explanations that can reconcile these results: first, the relative frequencies of La Niña and El Niño were similar between 1930 and 1970 when global temperature rise was small (Tsonis et al. 2005), and second that the dominant low-frequency period of ENSO shifted from 3–4 yr before 1910, to 4–7 yr between 1910 and 1960, and back to about 3 yr since the 1960s (Wang and Wang 1996; Moron et al. 1998). Hence, we can surmise that the connection between Atlantic cyclones and the tropical Pacific depends fundamentally on the specific mode of the ENSO dynamics.

e. Decadal variability

Figure 5 shows that on decadal scales TC is associated with SST variations over the Atlantic Gulf Stream and North Atlantic Drift region. Meandering of the Gulf Stream and variations in the northward transport of heat have been associated (Dijkstra and Ghil 2005) with 7.8-yr periodicity in the NAO; however, we find no coherence between TC and NAO. The Atlantic and Gulf Stream properties appear to have decadal to multi-decadal periodicity (Dijkstra and Ghil 2005; Bryden et al. 2005; Moses et al. 2006). High-frequency atmospheric forcing can lead to a low-frequency response in the coupled atmosphere–ocean system; moreover, feedbacks between the ocean and atmosphere may act in concert to amplify perturbations (Dijkstra and Ghil 2005). The effects of global warming on the meridional ocean heat transport are still poorly understood; how-

ever, the latest results (Bryden et al. 2005) suggest that more of the northward Gulf Stream flow was recirculating back southward than prior to the 1990s, and that northward heat transport across 25°N has dropped by 30% since 1990; hence, an increase in temperature over the MDR is likely. Also supporting this is the observation that decadal-scale SST oscillations do exhibit a dipole pattern between the North Atlantic Drift and Bahamas regions (Moron et al. 1998). From Fig. 4 we see that decadal power is associated with $m > 0$ and that increasing SST_C corresponds to more TCs. Thus, if global warming is responsible for both raising SST_C (Elsner 2006) and also reducing the efficiency of heat removal from the MDR via the Gulf Stream, then we would expect to see what is shown in Fig. 3: That the present is marked by strong coherence in the decadal period range.

In contrast with recent decades, the 1920–40 period was marked by coherence in the 5-yr scales and not at decadal ones, and with much less sensitivity between SST_C and TC. This would account for the nonstationarity found in analyzing high-resolution records of SST_C and storm events that do not take into account the long-period feedback mechanisms that become apparent on multiyear and decadal scales. The recently observed increasing correlation between SST_C and TC (Fig. 3) reflects the dominance of the decadal (Gulf Stream) mechanism and the weakness of the 5-yr (tropical atmospheric) mechanism.

5. Conclusions

Earlier work has identified statistical relationships between ENSO and Atlantic tropical cyclone genesis (Gray 1984), but there is no governing theory for long-term behavior. Here, we provide an analysis of the relationships between SST and storm count, which is a necessary step to understanding if a physical control exists.

Here, we introduce a novel method of analyzing time series relationships based on wavelets. The method has advantages over traditional regression or correlation analysis, most clearly in the case where one time series is lagged relative to the other. If we define causality to mean that significant predictions of a time series can be made knowing another time series (i.e., Granger causality), then we have shown that there is a causality link between tropical Atlantic SSTs and cyclone numbers.

Furthermore, we demonstrate that the August–October MDR SST and tropical cyclone numbers appear to be in a negative feedback loop on decadal time scales where rising SST_C leads to rising TC (with a sensitivity of two to four per degree Celsius), and that rising TC causes a decrease in the rate of increase of

SST_C. There are clear links on 5-yr periods between TC and ENSO activity, which appear to operate via an atmospheric rather than an oceanic SST bridge. This result is apparently confirmed by phase-aware teleconnections in the global SST and SLP fields, and is consistent with earlier findings that the increasing frequency of El Niño tends to reduce TC. However, on decadal time scales we find a link between TC and SST in the Gulf Stream and North Atlantic Drift region. The nature of this link is such that a decrease in heat transport northward leads to rising TC. The observed decrease in northward heat transport by the Gulf Stream (Bryden et al. 2005) appears to be dominating the increasing frequency of El Niño, as in recent decades the coherence between TC and SST_C is much stronger in the decadal than in the 5-yr bands. If global warming is responsible for the rise in SST_C and decreasing Gulf Stream heat transport, then there is a direct link between anthropogenic warming and increasing hurricane risk. This risk is enhanced because the Gulf Stream is effectively exporting less heat northward from the cyclone main development area than in previous decades; this effect is dominating the ameliorating effects of a warming tropical Pacific in reducing hurricane frequency. Thus, we show how the low-dimensional dynamics of the earth's climate system, represented by the Gulf Stream modulation of the thermohaline circulation, and the frequency of El Niño both significantly affect hurricane frequency.

Acknowledgments. Funding was provided by the Thule Institute and the Finnish Academy. Reviews from four anonymous referees provided many improvements to the manuscript.

REFERENCES

- Allan, R., and T. J. Ansell, 2006: A new globally complete monthly historical mean sea level pressure data set (HadSLP2): 1850–2004. *J. Climate*, **19**, 5816–5842.
- Bryden, H. L., H. R. Longworth, and S. A. Cunningham, 2005: Slowing of the Atlantic meridional overturning circulation at 25°N. *Nature*, **438**, 655–657, doi:10.1038/nature04385.
- Dijkstra, H. A., and M. Ghil, 2005: Low-frequency variability of the large-scale ocean circulation: A dynamical systems approach. *Rev. Geophys.*, **43**, RG3002, doi:10.1029/2002RG000122.
- Elsner, J. B., 2006: Evidence in support of the climate change–Atlantic hurricane hypothesis. *Geophys. Res. Lett.*, **33**, L16705, doi:10.1029/2006GL026869.
- Emanuel, K. A., 1986: An air–sea interaction theory for tropical cyclones. Part I: Steady-state maintenance. *J. Atmos. Sci.*, **43**, 585–604.
- , 1988: The maximum intensity of hurricanes. *J. Atmos. Sci.*, **45**, 1143–1155.
- , 2005: Increasing destructiveness of tropical cyclones over the past 30 years. *Nature*, **436**, 686–688.
- Goldenberg, S. B., C. W. Landsea, A. M. Mestas-Núñez, and W. M. Gray, 2001: The recent increase in Atlantic hurricane activity: Causes and implications. *Science*, **293**, 474–479.
- Granger, C. W. J., 1969: Investigating causal relations by econometric models and cross-spectral methods. *Econometrica*, **37**, 424–438.
- Gray, W. M., 1984: Atlantic seasonal hurricane frequency. Part I: El Niño and 30 mb quasi-biennial oscillation influences. *Mon. Wea. Rev.*, **112**, 1649–1668.
- Grinsted, A., J. C. Moore, and S. Jevrejeva, 2004: Application of the cross wavelet transform and wavelet coherence to geophysical time series. *Nonlinear Processes Geophys.*, **1**, 561–566.
- Jarvinen, B. R., C. J. Neumann, and M. A. D. Davis, 1984: A tropical cyclone data tape for the North Atlantic basin, 1886–1983: Contents, limitations, and uses. NOAA Tech. Memo. NWS NHC 22, 21 pp. [Available online at http://www.nhc.noaa.gov/tracks1851to2004_atl.txt.]
- Jevrejeva, S., and J. C. Moore, 2001: Singular spectrum analysis of Baltic Sea ice conditions and large-scale atmospheric patterns since 1708. *Geophys. Res. Lett.*, **28**, 4503–4506.
- Jones, P. D., T. Jonsson, and D. Wheeler, 1997: Extension using early instrumental pressure observations from Gibraltar and SW Iceland to the North Atlantic Oscillation. *Int. J. Climatol.*, **17**, 1433–1450.
- Kaplan, A., M. A. Cane, Y. Kushnir, A. C. Clement, M. B. Blumenthal, and B. Rajagopalan, 1998: Analyses of global sea surface temperature 1856–1991. *J. Geophys. Res.*, **103**, 18 567–18 589.
- Knutson, T. R., and R. E. Tuleya, 2004: Impact of CO₂-induced warming on simulated hurricane intensity and precipitation: Sensitivity to the choice of climate model and convective parameterization. *J. Climate*, **17**, 3477–3495.
- Landsea, C. W., 2005: Hurricanes and global warming. *Nature*, **438**, doi:10.1038/nature04477.
- , B. A. Harper, K. Hoarau, and J. A. Knaff, 2006: Can we detect trends in extreme tropical cyclones? *Science*, **313**, 452–454.
- Mann, M. E., and K. A. Emanuel, 2006: Atlantic hurricane trends linked to climate change. *Eos, Trans. Amer. Geophys. Union*, **87**, 233–244.
- , —, G. J. Holland, and P. J. Webster, 2007: Atlantic tropical cyclones revisited. *Eos, Trans. Amer. Geophys. Union*, **88**, 349–350.
- Michaels, P. J., P. C. Knappenberger, and R. E. Davis, 2006: Sea-surface temperatures and tropical cyclones in the Atlantic basin. *Geophys. Res. Lett.*, **33**, L09708, doi:10.1029/2006GL025757.
- Mokhov, I. I., and D. A. Smirnov, 2006: El Niño–Southern Oscillation drives North Atlantic Oscillation as revealed with nonlinear techniques from climatic indices. *Geophys. Res. Lett.*, **33**, L03708, doi:10.1029/2005GL024557.
- Moore, J. C., A. Grinsted, and S. Jevrejeva, 2006: Is there evidence for sunspot forcing of climate at multi-year and decadal periods? *Geophys. Res. Lett.*, **33**, L17705, doi:10.1029/2006GL026501.
- Moron, V., R. Vautard, and M. Ghil, 1998: Trends, interdecadal and interannual oscillations in global sea-surface temperatures. *Climate Dyn.*, **14**, 545–569.
- Moses, C. S., P. K. Swart, and B. E. Rosenheim, 2006: Evidence of multidecadal salinity variability in the eastern tropical North Atlantic. *Paleoceanography*, **21**, PA3010, doi:10.1029/2005PA001257.
- Rayner, N. A., and Coauthors, 2003: Global analyses of sea sur-

- face temperature, sea ice, and night marine air temperature since the late nineteenth century. *J. Geophys. Res.*, **108**, 4407, doi:10.1029/2002JD002670.
- Ropelewski, C. F., and P. D. Jones, 1987: An extension of the Tahiti–Darwin Southern Oscillation index. *Mon. Wea. Rev.*, **115**, 2161–2216.
- Smith, T. M., and R. W. Reynolds, 2004: Improved extended reconstruction of SST (1854–1997). *J. Climate*, **17**, 2466–2477.
- Torrence, C., and G. P. Compo, 1998: A practical guide to wavelet analysis. *Bull. Amer. Meteor. Soc.*, **79**, 61–78.
- Tsonis, A. A., J. B. Elsner, A. G. Hunt, and T. H. Jagger, 2005: Unfolding the relation between global temperature and ENSO. *Geophys. Res. Lett.*, **32**, L09701, doi:10.1029/2005GL022875.
- Wang, B., and Y. Wang, 1996: Temporal structure of the SOI as revealed by waveform and wavelet analysis. *J. Climate*, **9**, 1586–1598.
- Wang, C., D. B. Enfield, S. Lee, and C. W. Landsea, 2006: Influences of the Atlantic warm pool on Western Hemisphere summer rainfall and Atlantic hurricanes. *J. Climate*, **19**, 3011–3028.
- Zhang, Y., J. M. Wallace, and D. S. Battisti, 1997: ENSO-like interdecadal variability: 1900–93. *J. Climate*, **10**, 1004–1020.